Chaperonin GroEL accelerates protofibril formation and decorates fibrils of the Het-s prion protein

Marielle A. Wälti[a], Thomas Schmidt[a], Dylan T. Murray[a], Huaibin Wang[b], Jenny E. Hinshaw[b], and G. Marius Clore[a,1]

[a]Laboratory of Chemical Physics, National Institute of Diabetes and Digestive and Kidney Diseases, National Institutes of Health, Bethesda, MD 20892-0520; and [b]Laboratory of Cell and Molecular Biology, National Institute of Diabetes and Digestive and Kidney Diseases, National Institutes of Health, Bethesda, MD 20892-0820

Contributed by G. Marius Clore, July 13, 2017 (sent for review June 30, 2017; reviewed by James G. Omichinski and David J. Weber)

We have studied the interaction of the prototypical chaperonin GroEL with the prion domain of the Het-s protein using solution and solid-state NMR, electron and atomic force microscopies, and EPR. While GroEL accelerates Het-s protofibril formation by several orders of magnitude, the rate of appearance of fibrils is reduced. GroEL remains bound to Het-s throughout the aggregation process and densely decorates the fibrils at a regular spacing of ∼200 Å. GroEL binds to the Het-s fibrils via its apical domain located at the top of the large open ring. Thus, apo GroEL and bullet-shaped GroEL/GroES complexes in which only a single ring is capped by GroES interact with the Het-s fibrils; no evidence is seen for any interaction with football-shaped GroEL/GroES complexes in which both rings are capped by GroES. EPR spectroscopy shows that rotational motion of a nitroxide spin label, placed at the N-terminal end of the first β-strand of Het-s fibrils, is significantly reduced in both Het-s/GroEL aggregates and Het-s fibrils, but virtually completely eliminated in Het-s/GroEL fibrils, suggesting that in the latter, GroEL may come into close proximity to the nitroxide label. Solid-state NMR measurements indicate that GroEL binds to the mobile regions of the Het-s fibril comprising the N-terminal tail and a loop connecting β-strands 4 and 5, consistent with interactions involving GroEL binding consensus sequences located therein.

amyloid–chaperone interactions | NMR | EPR | electron microscopy | atomic force microscopy

The interaction of amyloids with chaperones, a group of proteins responsible for maintaining protein homeostasis (1–3), has attracted considerable attention with regard to the etiology of amyloidoses and accumulation of amyloid plaques (4). Diseases associated with amyloidosis include type II diabetes and a number of neurodegenerative processes such as Alzheimer's disease, Huntington disease, and spongiform encephalopathies (5).

Amyloids are unbranched, highly ordered protein aggregates that contain a cross β-structure arranged perpendicular to the fibril axis (6). Amyloid fibrils, which can be readily identified by electron microscopy, are formed by an ordered array of many copies of the given amyloid protein. In addition to amyloids that lead to pathology, there are amyloids where the fibrils contribute a distinct biological function (7). An example of the latter is provided by the Het-s prion protein from the filamentous fungus *Podospora anserina* (Fig. 1*A*) where Het-s fibril formation serves to prevent exchange of cytoplasmic material between genetically dissimilar species (5, 7). Since the structure of the Het-s fibril is well established (Fig. 1*B*) and not polymorphic at neutral pH (8, 9), and the Het-s monomer is stable for several days at 4 °C, we have used Het-s to study the interaction of a model amyloidogenic protein with a prototypical chaperone, GroEL, at the molecular and atomic levels.

GroEL is a member of the Hsp60 chaperonin class of chaperones, characterized by two cylindrically stacked heptameric ring structures, each enclosing a large interior cavity (or folding chamber) that encapsulates substrate proteins (Fig. 1*C*) (10). Although GroEL is a bacterial protein, Hsp60 chaperonins are structurally highly conserved throughout prokaryotes and eukaryotes: for example, *Escherichia coli* GroEL and human mitochondrial Hsp60 are 55% sequence identical (11). In eukaryotes, Hsp60s exist not only intracellularly where they play a key role in protein homeostasis, but also extracellularly where they function as potent stimulators of the immune response (12). Each GroEL subunit comprises three domains: equatorial, intermediate, and apical (10). The latter forms the rim around the entrance to the cavity and is responsible for binding both the cochaperone GroES and protein substrates.

Studying amyloid–chaperone interactions and their impact on protofibril and fibril formation is challenging because the species present during the early stages of fibril formation are heterogeneous. Recent work has shown that the formation of toxic amyloid species can be inhibited in a diverse manner by a range of chaperones (2, 13–21). This may involve inhibition of aggregation and protofibril formation (22), disaggregation (23, 24), or targeting misfolded proteins for rapid clearance (25). Biophysical data, however, on the interaction of chaperones with amyloid protofibrils and fibrils are relatively sparse, largely relying on fluorescence measurements tracking fibril formation.

Here, we make use of solution and solid-state NMR spectroscopy, electron (EM) and atomic force (AFM) microscopies, and electron paramagnetic resonance (EPR) spectroscopy to study the interaction of the prion forming domain (residues 218–289) of Het-s with GroEL at atomic resolution during the course of the complete aggregation pathway from monomer to complete fibril formation. We show that GroEL accelerates the formation of Het-s aggregates/protofibrils by orders of magnitude, eventually leading to the formation of fibrils densely decorated at regular intervals with GroEL. The interaction, which is already present at the protofibril stage,

Significance

The interaction of amyloids with chaperones, a large group of proteins responsible for proteostasis, is thought to play a significant role in the etiology of amyloidosis. Here, we study the interaction of the model chaperonin GroEL with a model amyloid protein, the prion domain of Het-s, by using NMR and EPR spectroscopies and electron and atomic force microscopies. We show that GroEL accelerates protofibril formation, eventually leading to the formation of fibrils densely decorated by GroEL. This type of chaperone–amyloid interaction may serve to reduce the toxicity of amyloidogenic oligomers and target the fully formed fibrils for rapid elimination by facilitating in vivo clearance.

Author contributions: M.A.W., T.S., D.T.M., J.E.H., and G.M.C. designed research; M.A.W., T.S., D.T.M., and H.W. performed research; M.A.W., T.S., D.T.M., J.E.H., and G.M.C. analyzed data; and M.A.W. and G.M.C. wrote the paper.

Reviewers: J.G.O., Université de Montréal; and D.J.W., University of Maryland School of Medicine.

The authors declare no conflict of interest.

[1]To whom correspondence should be addressed. Email: mariusc@intra.niddk.nih.gov.

This article contains supporting information online at www.pnas.org/lookup/suppl/doi:10.1073/pnas.1711645114/-/DCSupplemental.

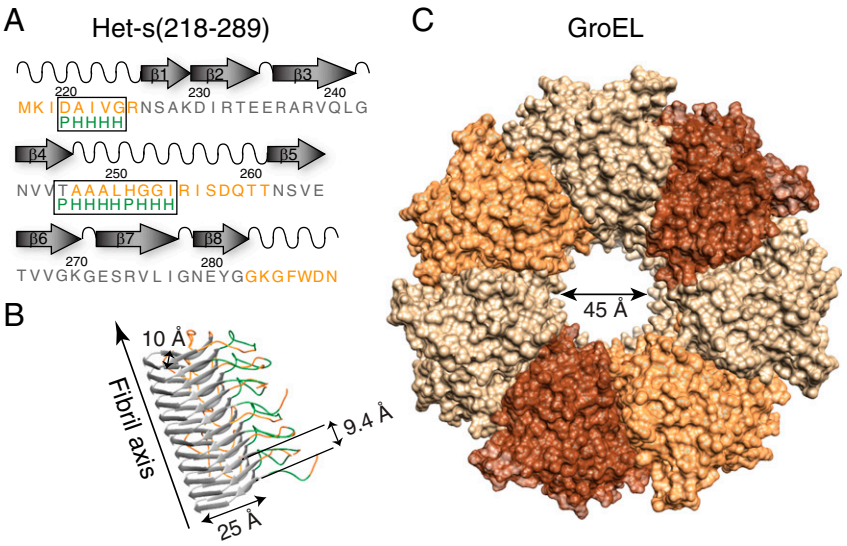

Fig. 1. Het-s(218–289) and GroEL. (*A*) Primary and secondary structure of Het-s(218–289) fibrils. Sequences within the flexible tails and loop are colored in orange, and the sites of GroEL-binding consensus sequences (a polar residue, P, followed by four hydrophobic residues, H) are indicated in green. (Note the N-terminal methionine is not part of the natural Het-s sequence.) (*B*) Structure of the Het-s(218–289) fibril determined by solid-state NMR (PDB ID code 2KJ3; ref. 9). (*C*) Structure of apo GroEL (PDB ID code 1XCK; ref. 41) showing a single heptameric ring viewed orthogonal to the long axis of the cavity. The structures in *B* and *C* are drawn to scale. Four to five Het-s(218–289) termini can potentially bind within each GroEL cavity.

occurs via the apical domain of GroEL and involves the mobile regions of Het-s.

Results and Discussion

Initial Aggregation. Addition of unlabeled GroEL (at natural isotopic abundance) to $^{1}H/^{15}N$-labeled Het-s(218–289) monomer results in an immediate (within the first 5 min), GroEL concentration-dependent decrease in cross-peak intensities in the ^{1}H-^{15}N correlation spectrum of monomeric Het-s (Fig. 2 *A* and *B*), accompanied by the appearance of protein aggregates or protofibrils as seen by both EM (Fig. 2 *C* and *D* and Fig. S1) and AFM (Fig. S1). At a ratio of 4 Het-s monomers per GroEL 14-mer (corresponding to the sample at 100 μM Het-s and 370 μM subunits of GroEL) only ∼4–5% Het-s monomer remains visible by NMR (Fig. 2*B*). Further, the concentration of GroEL required to reduce the fraction of NMR-visible Het-s monomer by 50% (i.e., 50% aggregation) is ∼5 μM GroEL 14-mer (∼70 μM in subunits) (Fig. 2*B*). SDS/PAGE indicates that the aggregates comprise both Het-s and GroEL (Fig. S2). In the absence of GroEL, Het-s remains monomeric for at least a day at room temperature with no EM evidence of protofibril formation.

Progression of Aggregation. We followed the disappearance of ^{15}N-labeled Het-s monomer as a function of time by solution NMR, monitoring overall signal intensity from the first increment of a ^{1}H-^{15}N correlation spectrum (Fig. 3*A*). Subsequent to the initial rapid decrease in monomer concentration occurring within the first 5 min after addition of GroEL as a result of protofibril formation (cf. Fig. 2 and Figs. S1 and S3*B*), there is a slow decrease in monomer concentration with a half-life of ∼2 d at GroEL concentrations of 10 and 50 μM (in subunits) and ∼2.7 d at 100 μM (in subunits) GroEL concentration. In the absence of GroEL, the decrease in Het-s monomer concentration is approximately mono-exponential with a half-life of approximately, 2.5 d (Fig. 3*A*). After 11–14 d at room temperature under quiescent conditions (i.e., not shaken or stirred), both protofibrils and fibrils are clearly seen in the EM and AFM images of the Het-s/GroEL samples (Fig. 3*B* and Fig. S3*D*); in the absence of GroEL only fibrils are seen by EM and AFM under the same conditions (Fig. 3*C* and Fig. S3*A*).

Characterization of Het-s/GroEL Fibrils by Electron Tomography. Electron tomograms taken 3 wk after addition of GroEL to Het-s reveals the presence of both multifilament fibril bundles (Fig. 4) and unifilament fibrils (Fig. 5) decorated in a regular,

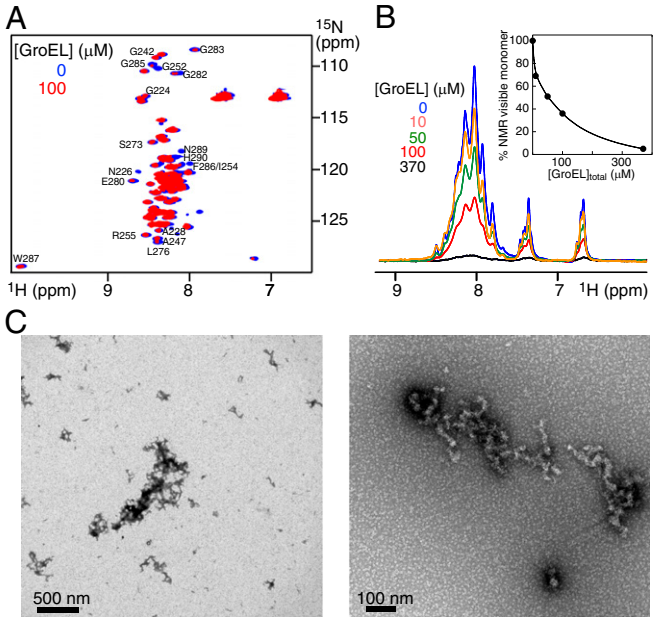

Fig. 2. GroEL concentration-dependent aggregation of Het-s(218–289) at time point zero. (*A*) ^{1}H-^{15}N HSQC spectra of 100 μM Het-s(218–289) alone (blue) and immediately after addition of 100 μM (in subunits) GroEL (red). (*B*) First increment of ^{1}H-^{15}N HSQC spectra acquired on 100 μM Het-s(218–289) in the presence of 0–370 μM (in subunits) GroEL at time point zero (i.e., recorded immediately after addition of GroEL). *Inset* shows a plot of the fractional decrease in NMR visible monomer as a function of total GroEL concentration (in subunits). (*C*) Electron micrographs of the Het-s aggregates (protofibrils, 100 μM in monomer units) formed immediately after addition of 100 μM (in subunits) GroEL at room temperature. In the same time frame, no aggregates/protofibrils are observed in the absence of GroEL addition.

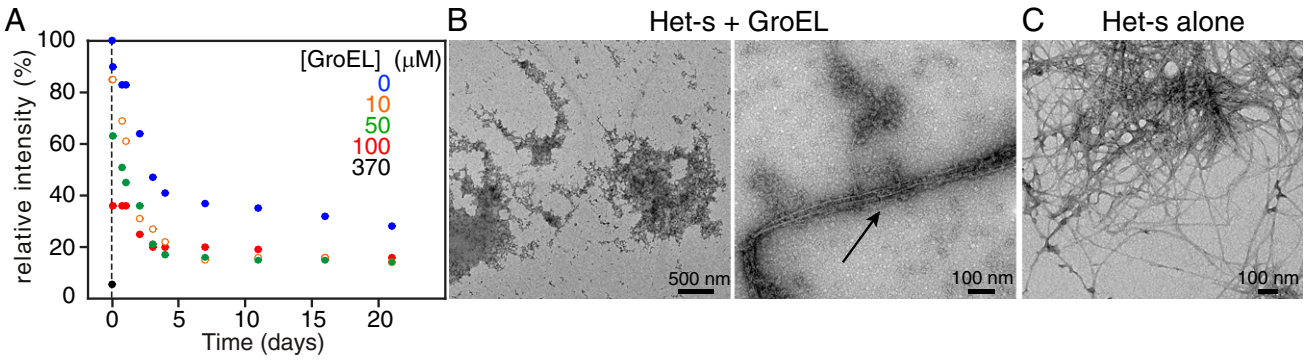

Fig. 3. Time dependence of Het-s(218–289) aggregation following addition of GroEL. (*A*) Disappearance of 100 μM Het-s(218–289) monomer over time as a function of GroEL concentration (specified in subunits), measured by solution-state NMR. (*B*) Electron micrographs of GroEL-induced Het-s protofibrils (*Left*) and fibrils (arrow, *Right*) obtained 11 d following the addition of 370 μM (in subunits) GroEL to 100 μM monomeric Het-s(218–289) at room temperature under quiescent conditions. (*C*) Het-s(218–289) fibrils obtained with 100 μM Het-s(218–289) alone at room temperature after 11 d under quiescent conditions.

densely packed manner by GroEL with a center-to-center spacing of ∼200 Å between adjacent bound GroEL molecules. GroEL binds on the lower (Fig. 4, *Left*), side (Fig. 4, *Center*) and upper (Fig. 4, *Right*) faces of the fibril bundles. The observation that GroEL is present on both sides of a unifilament fibril suggests that the filament twists in a helical manner about the long axis of the fibril (Fig. 5). Similar images are also observed when GroEL is added to preformed Het-s fibrils (Fig. 6 and see Fig. S5). Further magnification (Fig. 5) also reveals that GroEL binding to Het-s fibrils occurs exclusively via the open ring face of GroEL comprising a heptameric ring of apical domains (10).

The binding site on GroEL was confirmed by addition of GroEL/GroES complexes to preformed Het-s fibrils (Fig. 6*A*). GroES binds to the apical domain of GroEL, thereby capping either one or both GroEL rings (depending on conditions; see *Experimental Methods*) to form bullet-shaped (Fig. S4*A*) or football-shaped (Fig. S4*B*) complexes, respectively. In the resulting electron micrographs, the majority of GroEL particles bound to the Het-s fibrils is in the uncapped form (Fig. 6*B*, red boxes). Bullet-shaped GroEL/GroES complexes, however, are also clearly seen bound to the fibrils (Fig. 6*B*, blue boxes), but we see no evidence of any bound, football-shaped GroEL/GroES complexes (Fig. 6*B*, black boxes, and Fig. S5). Thus, binding of GroEL to Het-s fibrils requires the presence of at least one uncapped ring.

Characterization of Het-s Fibrils by Continuous Wave EPR. Continuous wave (CW) EPR spectroscopy provides a straightforward approach for probing the internal mobility of a nitroxide label [such as MTSL; (1-oxyl-2,2,5,5-tetramethyl-D3-pyrroline-3-methyl) methanethiosulfonate)]. We therefore MTSL-labeled Het-s(218–289) at position 227, located at the N terminus of strand β1, close to the disordered N-terminal tail (Fig. 1*A*), via an engineered cysteine mutation (S227C).

The lineshape of the EPR spectrum is sensitive to the mobility of the nitroxide label (26). At X-band, the EPR spectrum is dominated by the electron-nuclear hyperfine splitting tensor A. Rapid isotropic reorientation of the spin labels reduces the A tensor to a scalar value $a_{\mathrm{iso}} = 1/3(A_x + A_y + A_z)$, resulting in a three-line EPR spectrum with the two outer components separated by $2a_{iso}$; as rotational motion of the spin label is slowed down (or motion of the label hindered), the EPR lineshape changes, eventually reaching the powder limit in which the two outer components are separated by $2A_{zz}$ (27).

The CW X-band EPR spectrum of the nitroxide labeled Het-s(S227C) monomer is well described by an effective correlation time (τ_{eff}) of ∼0.5 ns (Fig. 7*A*). The EPR spectrum of Het-s fibrils formed in the absence of GroEL (Fig. 7*B*) and Het-s protofibrils formed immediately upon addition of GroEL (Fig. 7*C*) are characterized by a two-species system comprising a slow component with $\tau_{\mathrm{eff}} \sim 3.3$ ns corresponding to the fibrils and

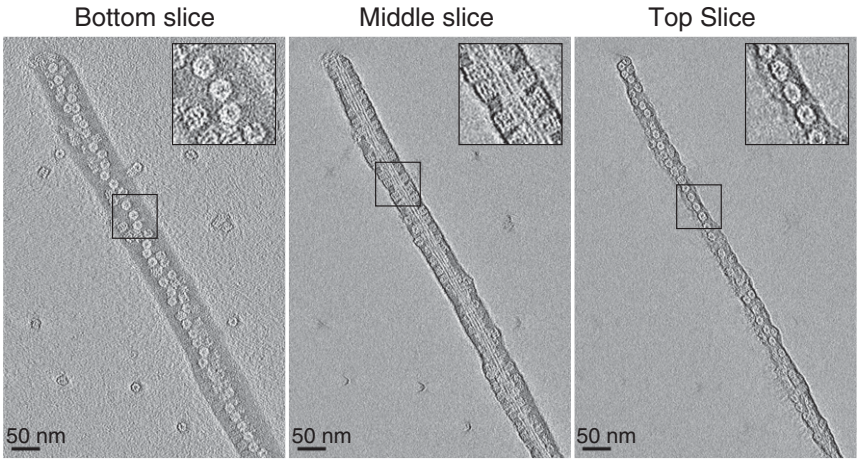

Fig. 4. Negative stain electron tomogram images of Het-s fibrils 3 wk after addition of 100 μM (in subunits) GroEL to 100 μM monomeric Het-s(218–289) at room temperature under quiescent conditions. All three slices clearly show that GroEL binds via its apical domain to the Het-s(218–289) fibrils. *Insets* show a zoom of a region of interest (black box).

Fig. 5. Regular spacing of GroEL bound via its apical domain to a Het-s monofilament. Shown is the middle slice of a negative stain electron tomogram image of a Het-s fibril formed 3 wk after addition of 100 μM (in subunits) GroEL to 100 μM Het-s(218–289) at room temperature under quiescent conditions. Also seen are three unbound GroEL molecules.

protofibrils, and a fast component $\tau_{eff} \sim 0.5$ ns corresponding to residual Het-s monomer present in the sample. The reduction in mobility of the nitroxide label in the fibrils and protofibrils can be attributed to the transition from a random coil to an ordered β-sheet structure containing the label. Finally, the EPR spectrum of the fibrils of Het-s formed in the presence of GroEL can be well reproduced by a three-species system comprising a powder ($\tau_{eff} >$ 200 ns or severely restricted motion with a high order parameter) characterized by the $2A_{zz}$ splitting (Fig. 7*D*), in addition to the two faster components seen in the Het-s fibrils alone and the Het-s/GroEL protofibrils. We attribute the powder species of the EPR spectrum to the immobilization of the nitroxide label attached to Het-s through direct interaction with GroEL, presumably binding to the GroEL-binding consensus sequences (28) located either in the N-terminal tail or the β4/β5 loop of Het-s fibrils (Fig. 1*A*). Many of the Het-s fibrils bound to GroEL consist of a multifilament bundle. Since GroEL binds to the outside of the fibrils, the nitroxide labels of only Het-s molecules in the outer filaments of the bundle can be fully immobilized by GroEL, accounting for the roughly equal population of the $\tau_{eff} \sim 3.3$ and >200 ns species in the EPR spectrum.

Solid-State NMR of Het-s Fibrils in the Presence of GroEL. To further characterize the interaction of GroEL with Het-s fibrils from the perspective of Het-s, we made use of solid-state NMR spectroscopy on uniformly $^{15}N/^{13}C$-labeled Het-s fibers grown in the absence and presence of GroEL (Fig. 8 and Figs. S6 and S7).

We first recorded a set of ^{1}H-^{13}C cross-polarization (CP)–based magic angle spinning (MAS) spectra, both 1D ^{13}C (Fig. 8*A*) and 2D $^{13}C/^{13}C$ with dipolar assisted rotational resonance (29) transfer between ^{13}C nuclei (Fig. S6). Under CP-MAS conditions, only rigid segments of the Het-s fibrils are probed (30). This is because molecular motions in dynamic regions prevent the dipolar coupling-based magnetization transfer used in CP-MAS–based experiments. The CP-MAS spectra of Het-s fibrils in the presence and absence of GroEL overlap perfectly, indicating that GroEL does not perturb the structure of the rigid fibril core.

Next, we recorded a set of 1D and 2D $^{1}H/^{13}C$ MAS spectra based on ^{1}H-^{13}C INEPT (insensitive nuclei enhanced by polarization transfer) transfers (Fig. 8 *B* and *C*) to probe the mobile regions of the Het-s fibrils (30), specifically, the N- and C-terminal tails and the long loop connecting β-strands 4 and 5. In INEPT-based experiments, magnetization is transferred from ^{1}H to ^{13}C via $^{1}J_{CH}$ scalar couplings, and ^{1}H and ^{13}C transverse relaxation rates must be longer than the time required for ^{1}H-^{13}C polarization transfer to observe a signal. In rigid segments of the protein with slow or anisotropic reorientations, the ^{1}H-^{1}H and ^{1}H-^{13}C dipolar couplings are not averaged to zero over time; in mobile regions, however, the dipolar interactions are time-averaged to zero, thereby eliminating the main mechanism of signal loss during INEPT transfer. Comparison of both the 1D (Fig. 8*B*) and 2D (Fig. 8*C*) $^{1}H/^{13}C$ INEPT spectra shows that the presence of GroEL results in significant differences. First, there is an obvious decrease in signal intensity in the 1D $^{1}H/^{13}C$ INEPT spectrum of Het-s fibrils with GroEL (Fig. 8*B*), accompanied by a corresponding decrease in the aliphatic ^{1}H and ^{13}C transverse relaxation times [from 24.7 ± 0.1 to 16.8 ± 0.1 ms, and from 4.8 ± 0.1 to 3.9 ± 0.2 ms, respectively (Fig. S7)]. Thus, one can conclude that GroEL binds to mobile and accessible segments of the Het-s fibrils. Further analysis of the 2D $^{1}H/^{13}C$ INEPT spectra reveals a few significant chemical shift differences as well, and the shifted cross-peaks can be assigned residue/atom type probabilities (31) (Fig. 8*C*). The latter are consistent with residues either in or close to the GroEL consensus-binding sequences (28) located in the N-terminal tail or β4/β5 loop (Fig. 8*C*).

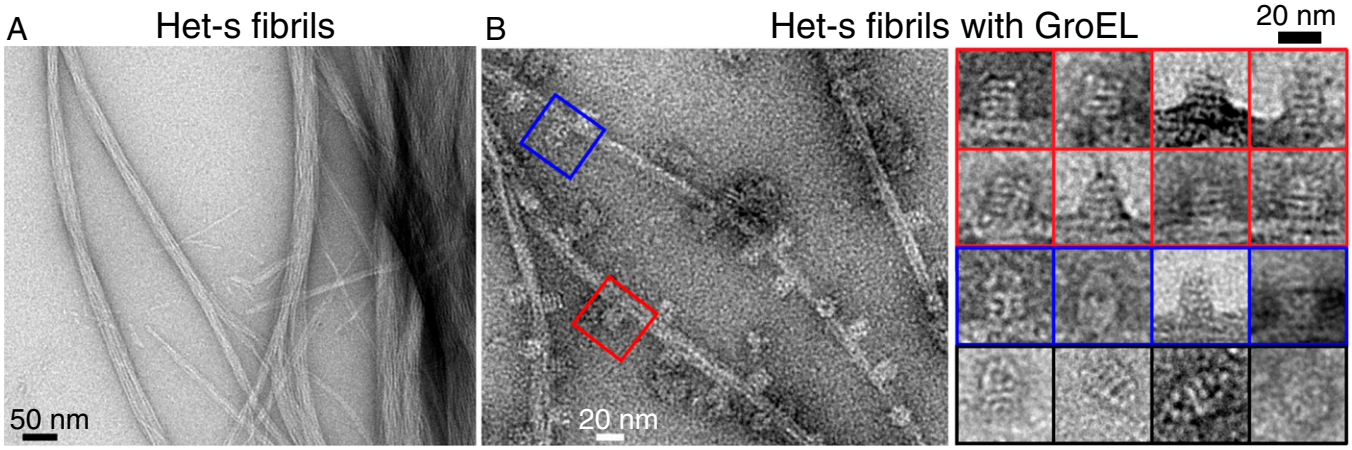

Fig. 6. Negative stain electron micrographs of Het-s fibrils formed in the absence (*A*) and presence (*B*) of GroEL and GroES. Most of the GroEL bound to Het-s is in the uncapped form (red box); however, some bullet-shaped GroEL/GroES complexes are also bound to the Het-s fibrils (blue box). *Right* images show a collection of enlarged micrographs of differently prepared samples where uncapped bound GroEL (first and second rows, red), bullet-shaped bound GroEL/GroES complexes (third row, blue), and unbound football-shaped GroEL/GroES complexes (fourth row, black) are found. One hundred micromolar Het-s(218–289) was fibrilized for 3 wk at room temperature under quiescent conditions. Bullet- or football-shaped GroEL/GroES complexes (prepared as described in *Experimental Methods*) were mixed separately with Het-s fibrils leading to micrographs shown in the blue or black boxes (*B, Right*), respectively (see also Fig. S5).

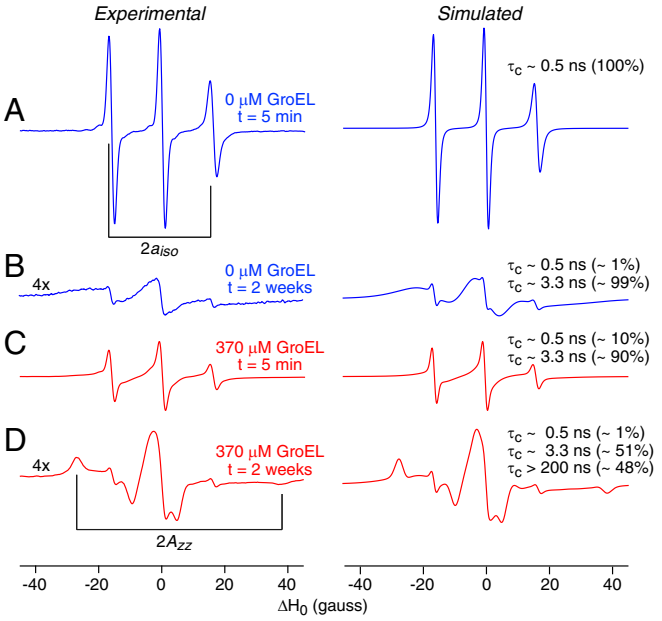

Fig. 7. Comparison of experimental and simulated CW X-band EPR spectra of MTSL-labeled Het-s (S227C) in different states. (*A*) Monomeric Het-s. (*B*) Het-s fibrils were obtained after 2 wk at room temperature, centrifuged, and the pellet was resuspended in water (*C*) Het-s protofibrils obtained within 5 min of addition of GroEL (the sample is not spun down). (*D*) Het-s fibrils obtained at room temperature 2 wk after the addition of GroEL, centrifuged, and the pellet was resuspended in water. The experimental and simulated first derivative EPR spectra are shown in the left and right columns, respectively. The simulated spectra were calculated with different correlation times and species populations as indicated (26). The derivative EPR spectra are normalized to the double integral.

Concluding Remarks

Using a range of biophysical and structural techniques, we have shown that the chaperonin GroEL interacts directly with the Het-s prion protein, resulting in a two order of magnitude or larger speed up of aggregation and protofibril formation. The rate of appearance of fully formed fibrils, however, is slowed down in the presence of GroEL. Thus, after 11 d, both protofibils and fibrils of Het-s are seen in the presence of GroEL (Fig. 3*B*), while only fibrils are observed for Het-s alone (Fig. 3*C*). After 3 wk, however, the Het-s protofibrils obtained in the presence of GroEL have largely been converted to fibrils. GroEL remains bound to Het-s throughout the aggregation process and decorates Het-s fibrils with a regular spacing of ~200 Å. Given the diameter of the GroEL cavity, we surmise that GroEL interacts with four to five Het-s units within a fibril, thereby resulting in high avidity.

The interaction of GroEL with amyloid-type fibrils, in this instance Het-s, requires that mobile regions within the fibril (containing one or more GroEL consensus binding sequences) be able to access the inner rim of the central cavity of GroEL formed by the apical domain. Thus, amyloid fibrils without these particular characteristics would not be expected to interact with GroEL in the same manner as Het-s. For example, while GroEL binds to amyloid-β monomers via two GroEL-binding consensus sequences (32), these sequences are largely located in ordered β-sheet regions of the fibril (33–35). Hence, one would predict that interaction between GroEL and amyloid-β fibrils would only occur upon disruption of the fibril.

In the context of the etiology of amyloidosis, the type of interaction seen here between GroEL and Het-s protofibrils and fibrils may serve two functions. First, chaperone binding to toxic amyloid oligomers may render these nontoxic by sequestration into large aggregates, as has been demonstrated in the case of the interaction between the small heat shock protein HspB1 and amyloid-β protofibrils (36). Second, binding of chaperones to fully formed fibrils may facilitate in vivo clearance (e.g., in the liver) as was shown for the extracellular chaperone clusterin (25).

Experimental Methods

Expression and Purification. Details of the expression and purification of GroEL, GroES, and Het-s(218–289) are provided in *SI Experimental Methods*. GroEL/GroES bullet-shaped and football-shaped complexes in which one or both GroEL rings are capped, respectively, were prepared essentially as described with some minor modifications (37). Fibrillization of Het-s(218–289) was carried out as described (38).

NMR and EPR Spectroscopy. Solution NMR measurements were carried out on a Bruker 600 MHz NMR spectrometer with a triple resonance *z* axis gradient cryoprobe at 10 °C. Further details are provided in *SI Experimental Methods*. Solid-state NMR was carried out on a 17.5 T spectrometer (^{1}H frequency of 746 MHz) using a Chemmagnetics console and a Black Fox magic angle spinning probe with 12 kHz spinning. Details of the ^{1}H-^{13}C CP and INEPT experiments

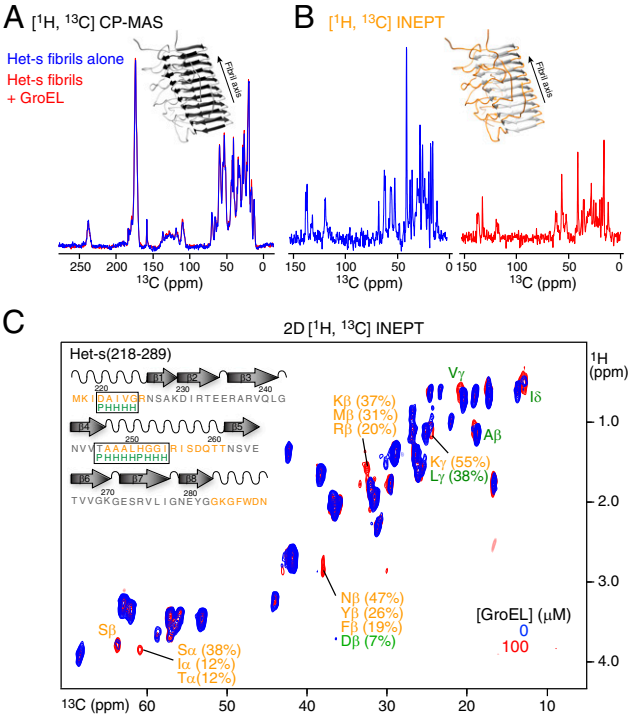

Fig. 8. Solid-state NMR of Het-s fibrils formed in the presence and absence of GroEL. Comparison of 1D [^{1}H, ^{13}C] CP-MAS (*A*) and [^{1}H, ^{13}C] INEPT-MAS (*B*) spectra of Het-s fibrils formed in the absence (blue) and presence (red) of GroEL. *Insets* shows the structure of a Het-s(218–289) fibril (PDB ID code 2RNM; ref. 8) with the rigid portions colored in dark gray (*A*) and the mobile tails and loops in orange (*B*). (*C*) Comparison of 2D [^{1}H,^{13}C] INEPT-MAS spectra of Het-s fibrils formed in the absence (blue) and presence (red) of GroEL. The 1D CP-based spectra (*A*) overlap perfectly showing that the rigid segments (dark gray) of the Het-s(218–289) fibrils have the same overall structure in presence and absence of GroEL, confirmed by the 2D [^{13}C,^{13}C] Dipolar Assisted Rotational Resonance (DARR) spectra shown in Fig. S6). There are large differences in peak intensities in the INEPT-based experiments (*B* and *C*) indicating differences in the mobile portions of the fibrils upon GroEL binding. Cross-peaks of Het-s fibrils with significant chemical shift differences in the presence and absence of GroEL, together with assignments in terms of residue/atom type probabilities (31), are indicated. One hundred micromolar monomeric Het-s(218–289) was fibrilized at room temperature under quiescent conditions in the absence and presence of 100 μM (in subunits) GroEL.

are provided in *SI Experimental Methods*. CW EPR spectra at X-band were recorded on a Bruker EMX spectrometer (see *SI Experimental Methods*).

EM and AFM. Samples of Het-s/GroEL complexes were prepared in the same manner as for the solution-state NMR experiments (*SI Experimental Methods*). Aliquots were taken at different time points and diluted to a final GroEL concentration of 2.5 μM. For EM, 5-μL samples were blotted onto the carbon-coated copper EM grids (Ultrathin Carbon Film/Holey Carbon; Ted Pella) for 1 min, quickly washed with deionized water, and stained with 2% uranyl acetate for 40 s. Images were taken with an FEI Tecnai T12 electron microscope operating at 120 kV and a Gatan US1000 CCD camera.

For electron tomography, tilt series were collected using SerialEM (39) on an FEI Tecnai F20 electron microscope operating at 200 kV and equipped with a Gatan K2 direct electron detector. The tilt series ranges from –60 to +60 degrees in increments of 2 degrees. Tomograms were reconstructed using the ETomo routine in the IMOD package (40).

For AFM, the same samples were directly applied to freshly cleaved mica. The sample was incubated for 1 min, washed with deionized water, and further air dried. AFM images were taken in the tapping mode using a MultiMode AFM with a Nanoscope IV controller (Veeco). This included a SPM probe model ACT silicon (Applied Nanostructures) with a 5- to 6-nm tip radius, 40 N/m force constant, and oscillating at ≈300 kHz. Images were recorded at a scan rate of 0.7–1 Hz, 256 sampling points per line, and 256 lines.

ACKNOWLEDGMENTS. We thank Rob Tycko for useful discussions; James Baber, Dan Garrett, and Jinfa Ying for technical support; and Roland Riek for the gift of the Het-s(218–289) clone. M.A.W. was supported by an Early Postdoc.Mobility Fellowship from the Swiss National Science Foundation. D.T.M. was supported by the Postdoctoral Research Associate Program of the National Institute of General Medical Sciences, NIH Award Fi2GM117604. This work was supported by the Intramural Program of the National Institute of Diabetes and Digestive and Kidney Diseases, National Institutes of Health (G.M.C. and J.E.H.), and by the AIDS-Targeted Antiviral Program of the Office of the Director of the National Institutes of Health (G.M.C.).

1. Hartl FU, Hayer-Hartl M (2002) Molecular chaperones in the cytosol: From nascent chain to folded protein. *Science* 295:1852–1858.
2. Balch WE, Morimoto RI, Dillin A, Kelly JW (2008) Adapting proteostasis for disease intervention. *Science* 319:916–919.
3. Hartl FU, Bracher A, Hayer-Hartl M (2011) Molecular chaperones in protein folding and proteostasis. *Nature* 475:324–332.
4. Wyatt AR, Yerbury JJ, Dabbs RA, Wilson MR (2012) Roles of extracellular chaperones in amyloidosis. *J Mol Biol* 421:499–516.
5. Chiti F, Dobson CM (2006) Protein misfolding, functional amyloid, and human disease. *Annu Rev Biochem* 75:333–366.
6. Eanes ED, Glenner GG (1968) X-ray diffraction studies on amyloid filaments. *J Histochem Cytochem* 16:673–677.
7. Fowler DM, Koulov AV, Balch WE, Kelly JW (2007) Functional amyloid—from bacteria to humans. *Trends Biochem Sci* 32:217–224.
8. Wasmer C, et al. (2008) Amyloid fibrils of the HET-s(218-289) prion form a β solenoid with a triangular hydrophobic core. *Science* 319:1523–1526.
9. Van Melckebeke H, et al. (2010) Atomic-resolution three-dimensional structure of HET-s(218-289) amyloid fibrils by solid-state NMR spectroscopy. *J Am Chem Soc* 132: 13765–13775.
10. Braig K, et al. (1994) The crystal structure of the bacterial chaperonin GroEL at 2.8 A. *Nature* 371:578–586.
11. Zeilstra-Ryalls J, Fayet O, Georgopoulos C (1991) The universally conserved GroE (Hsp60) chaperonins. *Annu Rev Microbiol* 45:301–325.
12. Pei W, et al. (2016) Extracellular HSP60 triggers tissue regeneration and wound healing by regulating inflammation and cell proliferation. *NPJ Regenerative Med*, 16013.
13. Muchowski PJ, Wacker JL (2005) Modulation of neurodegeneration by molecular chaperones. *Nat Rev Neurosci* 6:11–22.
14. Jones GW, Tuite MF (2005) Chaperoning prions: The cellular machinery for propagating an infectious protein? *BioEssays* 27:823–832.
15. Dedmon MM, Christodoulou J, Wilson MR, Dobson CM (2005) Heat shock protein 70 inhibits alpha-synuclein fibril formation via preferential binding to prefibrillar species. *J Biol Chem* 280:14733–14740.
16. Knowles TP, et al. (2007) Kinetics and thermodynamics of amyloid formation from direct measurements of fluctuations in fibril mass. *Proc Natl Acad Sci USA* 104: 10016–10021.
17. Perrett S, Jones GW (2008) Insights into the mechanism of prion propagation. *Curr Opin Struct Biol* 18:52–59.
18. Zhang H, Xu LQ, Perrett S (2011) Studying the effects of chaperones on amyloid fibril formation. *Methods* 53:285–294.
19. Shammas SL, et al. (2011) Binding of the molecular chaperone α_B-crystallin to Aβ amyloid fibrils inhibits fibril elongation. *Biophys J* 101:1681–1689.
20. Mannini B, et al. (2012) Molecular mechanisms used by chaperones to reduce the toxicity of aberrant protein oligomers. *Proc Natl Acad Sci USA* 109:12479–12484.
21. Månsson C, et al. (2014) DNAJB6 is a peptide-binding chaperone which can suppress amyloid fibrillation of polyglutamine peptides at substoichiometric molar ratios. *Cell Stress Chaperones* 19:227–239.
22. Arosio P, et al. (2016) Kinetic analysis reveals the diversity of microscopic mechanisms through which molecular chaperones suppress amyloid formation. *Nat Commun* 7:10948.
23. Mogk A, Bukau B (2004) Molecular chaperones: Structure of a protein disaggregase. *Curr Biol* 14:R78–R80.
24. Doyle SM, Genest O, Wickner S (2013) Protein rescue from aggregates by powerful molecular chaperone machines. *Nat Rev Mol Cell Biol* 14:617–629.
25. Wyatt AR, et al. (2011) Clusterin facilitates in vivo clearance of extracellular misfolded proteins. *Cell Mol Life Sci* 68:3919–3931.
26. Stoll S, Schweiger A (2006) EasySpin, a comprehensive software package for spectral simulation and analysis in EPR. *J Magn Reson* 178:42–55.
27. Nesmelov YE, Thomas DD (2010) Protein structural dynamics revealed by site-directed spin labeling and multifrequency EPR. *Biophys Rev* 2:91–99.
28. Stan G, Brooks BR, Lorimer GH, Thirumalai D (2006) Residues in substrate proteins that interact with GroEL in the capture process are buried in the native state. *Proc Natl Acad Sci USA* 103:4433–4438.
29. Takegoshi K, Nakamura S, Terao T (2003) ^{13}C-^{1}H dipolar-driven ^{13}C-^{13}C recoupling without ^{13}C rf irradiation in nuclear magnetic resonance of rotating solids. *J Chem Phys* 118:2325–2341.
30. Sackewitz M, et al. (2008) Structural and dynamical characterization of fibrils from a disease-associated alanine expansion domain using proteolysis and solid-state NMR spectroscopy. *J Am Chem Soc* 130:7172–7173.
31. Vranken WF, et al. (2005) The CCPN data model for NMR spectroscopy: Development of a software pipeline. *Proteins* 59:687–696.
32. Libich DS, Fawzi NL, Ying J, Clore GM (2013) Probing the transient dark state of substrate binding to GroEL by relaxation-based solution NMR. *Proc Natl Acad Sci USA* 110:11361–11366.
33. Lührs T, et al. (2005) 3D structure of Alzheimer's amyloid-β(1-42) fibrils. *Proc Natl Acad Sci USA* 102:17342–17347.
34. Paravastu AK, Leapman RD, Yau WM, Tycko R (2008) Molecular structural basis for polymorphism in Alzheimer's β-amyloid fibrils. *Proc Natl Acad Sci USA* 105: 18349–18354.
35. Wälti MA, et al. (2016) Atomic-resolution structure of a disease-relevant Aβ(1-42) amyloid fibril. *Proc Natl Acad Sci USA* 113:E4976–E4984.
36. Ojha J, Masilamoni G, Dunlap D, Udoff RA, Cashikar AG (2011) Sequestration of toxic oligomers by HspB1 as a cytoprotective mechanism. *Mol Cell Biol* 31:3146–3157.
37. Taguchi H, Tsukuda K, Motojima F, Koike-Takeshita A, Yoshida M (2004) BeF(x) stops the chaperonin cycle of GroEL-GroES and generates a complex with double folding chambers. *J Biol Chem* 279:45737–45743.
38. Daskalov A, et al. (2014) Contribution of specific residues of the β-solenoid fold to HET-s prion function, amyloid structure and stability. *PLoS Pathog* 10:e1004158.
39. Mastronarde DN (2005) Automated electron microscope tomography using robust prediction of specimen movements. *J Struct Biol* 152:36–51.
40. Kremer JR, Mastronarde DN, McIntosh JR (1996) Computer visualization of three-dimensional image data using IMOD. *J Struct Biol* 116:71–76.
41. Bartolucci C, Lamba D, Grazulis S, Manakova E, Heumann H (2005) Crystal structure of wild-type chaperonin GroEL. *J Mol Biol* 354:940–951.
42. Grason JP, Gresham JS, Widjaja L, Wehri SC, Lorimer GH (2008) Setting the chaperonin timer: The effects of K^+ and substrate protein on ATP hydrolysis. *Proc Natl Acad Sci USA* 105:17334–17338.
43. Todd MJ, Lorimer GH (1998) Criteria for assessing the purity and quality of GroEL. *Methods Enzymol* 290:135–141.
44. Ritter C, et al. (2005) Correlation of structural elements and infectivity of the HET-s prion. *Nature* 435:844–848.
45. Chaudhry C, Horwich AL, Brunger AT, Adams PD (2004) Exploring the structural dynamics of the E.coli chaperonin GroEL using translation-libration-screw crystallographic refinement of intermediate states. *J Mol Biol* 342:229–245.
46. Fei X, Ye X, LaRonde NA, Lorimer GH (2014) Formation and structures of GroEL: $GroES_2$ chaperonin footballs, the protein-folding functional form. *Proc Natl Acad Sci USA* 111:12775–12780.